

WGS Catalysis and In Situ Studies of CoO_{1-x} , $\text{PtCo}_n/\text{Co}_3\text{O}_4$, and $\text{Pt}_m\text{Co}_{m'}/\text{CoO}_{1-x}$ Nanorod Catalysts

Shiran Zhang,^{†,||} Jun-jun Shan,^{†,||} Yuan Zhu,^{†,||} Anatoly I. Frenkel,[‡] Anitha Patlolla,[‡] Weixin Huang,[†] Seog Joon Yoon,[†] Lei Wang,[†] Hideto Yoshida,[§] Seiji Takeda,[§] and Franklin (Feng) Tao^{†,*}

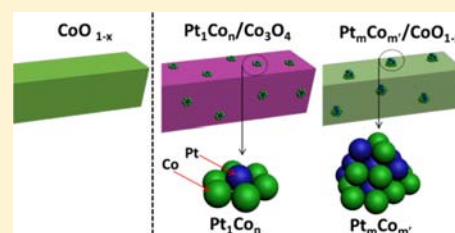
[†]Department of Chemistry and Biochemistry, University of Notre Dame, Notre Dame, Indiana 46556, United States

[‡]Department of Physics, Yeshiva University, New York, New York 10016, United States

[§]Institute of Scientific and Industrial Research, Osaka University, 8-1 Mihogaoka, Ibaraki, Osaka 567-0047, Japan

Supporting Information

ABSTRACT: Water–gas shift (WGS) reactions on Co_3O_4 nanorods and Co_3O_4 nanorods anchoring singly dispersed Pt atoms were explored through building correlation of catalytic performance to surface chemistry of catalysts during catalysis using X-ray absorption spectroscopy, ambient pressure X-ray photoelectron spectroscopy (AP-XPS), and environmental TEM. The active phase of pure Co_3O_4 during WGS is nonstoichiometric cobalt monoxide with about 20% oxygen vacancies, $\text{CoO}_{0.80}$. The apparent activation energy (E_a) in the temperature range of 180–240 °C is $91.0 \pm 10.5 \text{ kJ mol}^{-1}$. Co_3O_4 nanorods anchoring Pt atoms ($\text{Pt}/\text{Co}_3\text{O}_4$) are active for WGS with a low E_a of $50.1 \pm 5.0 \text{ kJ mol}^{-1}$ in the temperature range of 150–200 °C. The active surface of this catalyst is singly dispersed Pt_1Co_n nanoclusters anchored on Co_3O_4 ($\text{Pt}_1/\text{Co}_3\text{O}_4$), evidenced by in situ studies of extended X-ray absorption fine structure spectroscopy. In the temperature range of 200–300 °C, catalytic in situ studies suggested the formation of $\text{Pt}_m\text{Co}_{m'}$ nanoclusters along with the reduction of Co_3O_4 substrate to CoO_{1-x} . The new catalyst, $\text{Pt}_m\text{Co}_{m'}/\text{CoO}_{1-x}$ is active for WGS with a very low E_a of $24.8 \pm 3.1 \text{ kJ mol}^{-1}$ in the temperature range of 300–350 °C. The high activity could result from a synergy of $\text{Pt}_m\text{Co}_{m'}$ nanoclusters and surface oxygen vacancies of CoO_{1-x} .



1. INTRODUCTION

Water–gas shift (WGS) catalysis with high activity at a temperature near the operational temperature of low-temperature fuel cells is one solution for on-board purification of hydrogen sources for low-temperature fuel cell technology, since the CO tolerance of fuel cell electrodes is only 50 ppm or lower.^{1–5} Development of catalysts with high activity at low temperatures has driven significant effort toward fundamental studies of low-temperature WGS on catalysts distinct from industrial Cu and Fe WGS catalysts.^{6–8} Noble metals, including Au and Pt impregnated on CeO_2 and TiO_2 , have been extensively studied in recent decades.^{9–28} They catalyze WGS through a bifunctional mechanism. Both the metal and oxygen vacancies of reducible oxides play a synergic role in WGS.^{18,26,29,30} It is generally acknowledged that metal particles adsorb CO and oxygen vacancies dissociate H_2O molecules to form OH groups. The adsorbed CO molecules couple with the formed OH at the oxide–metal interface, forming an intermediate which reforms and dissociates into CO_2 and a hydrogen atom. This hydrogen atom spills over and couples with another hydrogen atom to form a hydrogen molecule.

Co_3O_4 is a reducible oxide of an early transition metal. It exhibits extraordinarily high activity in CO oxidation even at -77 °C, due to the weaker bond strength of Co–O and low hopping barrier of oxygen vacancies on the surface, in contrast to most other oxides of the 3d transition metals.^{31,32} It has been

confirmed that different types of oxygen vacancies play different roles in adsorbing oxygen molecules and dissociating them to provide active oxygen atoms.³³ So far, there has been no conclusive assignment of the active sites and mechanism for CO oxidation on Co_3O_4 .³³

Cobalt oxides exist in three different structures, including Co_3O_4 with spinel structure, CoO with rocksalt structure, and Co_2O_3 with hexagonal structure. Co_3O_4 is the thermodynamically favorable phase at room temperature. However, it can be reduced to rocksalt CoO by annealing it in a reducing gas or even just in an ultrahigh high vacuum. In terms of Co_2O_3 , it is not chemically stable, and thus it is challenging to prepare.^{34,35} Co_3O_4 exhibits distinctly different packing of the oxygen and cobalt atoms in terms of the crystallographic lattice, in contrast to CoO. Bond lengths of Co(II)–O (1.99 Å) and Co(III)–O (1.89 Å) of Co_3O_4 ^{23,36} are slightly shorter than that of the Co(II)–O of CoO (2.13 Å),³⁷ suggesting a weaker Co–O bond of CoO. The low barrier for the hopping of oxygen vacancies³⁸ on the Co_3O_4 surface shows a high mobility of surface lattice oxygen atoms, making it readily generate oxygen vacancies. It further indicates a higher mobility of oxygen atoms on CoO, in contrast to Co_3O_4 . Inspired by (1) the role of the oxygen vacancies of the CeO_2 and TiO_2 surface in WGS on Au

Received: February 23, 2013

Published: April 23, 2013

(or Pt)/CeO₂ (or TiO₂)^{6,7} and (2) the lowest dissociation energy of the M–O bond (M: metal) of cobalt oxides,¹⁰ we hypothesized that cobalt oxide could be a good component for a catalyst in a low-temperature WGS reaction, since it can generate oxygen vacancies readily and its surface lattice oxygen can adsorb CO molecules.³³ As oxygen vacancies can be generated on Co₃O₄³¹ or CoO under certain conditions, a bifunctional catalyst based on Co₃O₄ or CoO could be developed. As the mobility of surface lattice oxygen atoms on cobalt oxide is much larger than that on TiO₂ or CeO₂,³⁸ active metals such as Pt could be anchored on Co₃O₄ during generation of oxygen vacancies in calcination. Thus, cobalt oxide anchoring Pt atoms could be developed. It could offer different catalytic performances in contrast to Pt/CeO₂ and Pt/TiO₂ since surface lattice oxygen atoms of Co₃O₄ or CoO exhibit high mobility and Co₃O₄ could be transformed to CoO_{1-x}.

Here we synthesized pure Co₃O₄ nanorods and Co₃O₄ anchoring Pt atoms. In situ extended X-ray absorption fine structure (EXAFS) measurements established evidence that Pt atoms are dispersed as single atoms on the cobalt oxide support. Their surface chemistry at different temperatures was characterized with ambient pressure XPS (AP-XPS) while a catalyst is placed in a flow reactor installed in AP-XPS. Correlations between catalytic in situ surface chemistry of catalysts during catalysis and their kinetics were built. The as-synthesized Co₃O₄ (nominal catalyst) is active for WGS. AP-XPS studies revealed that the active phase of the nominal catalyst, Co₃O₄ in WGS, is in fact CoO_{1-x}. In situ studies showed that the as-synthesized Pt/Co₃O₄ is restructured to Pt₁Co_n/Co₃O₄ which is active for WGS in the temperature regime of 150–200 °C with E_a of 50.1 ± 5.0 kJ mol⁻¹. Pt₁Co_n/Co₃O₄ is further restructured in the temperature range of 200–300 °C, forming a different active phase, Pt_mCo_m/CoO_{1-x}. This new phase exhibits high activity at 300–350 °C with an E_a of 24.8 ± 3.1 kJ mol⁻¹.

2. EXPERIMENTAL SECTION

Co₃O₄ nanorods were synthesized with a hydrothermal method. Cobalt acetate tetrahydrate is used as the synthetic precursor. It undergoes a hydrogenolysis process when dissolved in ethylene glycol due to the considerably large molecular ratio of ethylene glycol to water. After the introduction of the sodium carbonate solution, the amount of water molecules increases and triggers hydrolysis along with the attendant fast nucleation of the precursors. The precursors then form layered structures with edge-sharing coordination of hydroxide anions, analogous to the layered double hydroxides, which further form sheet-like structures by self-assembly due to the interlaying hydrogen bonds between the acetates and the hydroxides. Carbonate anions were added to serve as the structure-directing agent. As there are more Co²⁺ in the (110) plane, the recrystallization will be inhibited by the coordination of Co²⁺ to carbonate anions, which gives rise to the preferential exposure of (110) plane. In the aging stage, ethylene glycol is incorporated into the structure by replacing both carbonates and acetates. It largely influences crystalline aggregation and promotes formation of a network of small interconnected pores. Ethylene glycol further contributes to the disintegration of the remaining sheet-like structures and fulfills the formation of pristine nanorods in solution. The pristine nanorods are then washed with deionized water and ethanol and then calcined at 300–450 °C in air for 4 h.

For synthesis of Pt/Co₃O₄ catalyst, Pt was anchored on the surface of well crystallized Co₃O₄ nanorods with deposition-precipitation.³⁹ There is no significant change of size and surface morphology in Co₃O₄ upon anchoring Pt ions. The Pt/Co₃O₄ weight ratio is 0.5% based on the measurements using inductively coupled plasma analysis

(ICP) at our Centre for Environmental Science and Technology. The morphology of catalysts was identified with Titan TEM (FEI Titan 80–300, 300 kV FEG TEM with point resolution 0.2 Å). HAADF-STEM images were collected on JEOL JEM-ARM 200F with a CEOS probe corrector in Takeda group at Osaka University at Japan. The used accelerating voltage is 200 kV. The HAADF-STEM resolution is 0.1 nm.

Surface chemistry of the two different nominal catalysts (Co₃O₄ or Pt/Co₃O₄) before catalysis or any pretreatment was characterized with XPS in ultrahigh vacuum (UHV). Au thin film (0.4-mm thick, 99.99%, VWR) was used as a substrate to load a catalyst. Au foil was deliberately roughened using an SiC knife to increase adhesion. A certain amount of catalyst powder is dispersed into ethanol to prepare an original solution. This solution was further diluted with ethanol to a concentration such that a single layer of nanorods of catalyst (Co₃O₄ or Pt/Co₃O₄ nanorods) can be prepared by dropping a small droplet of the diluted solution on Au substrate. This concentration can be calculated from the size of Co₃O₄ nanorods and the size of Au substrate. Ethanol left in the thin layer on the Au foil is vaporized by placing Au foil in a vacuum oven at 60 °C. A dry Au sample with a layer of physically adsorbed nanorods is ready for XPS studies. Such a preparation of sample for XPS studies can effectively minimize surface charging resulting from thick catalyst layers. The apparent binding energies of Au 4f, Co 2p, and O 1s of sample prepared with the above method are very close to their real values, suggesting there is no obvious surface charging. The offset is typically smaller than 0.1–0.2 eV. Characterization of surface chemistry before catalysis was performed on the ambient pressure XPS system, since it acts as a high vacuum XPS while there is no gas introduced into the catalytic reactor. Au 4f_{7/2} was always collected immediately upon scanning Co 2p and O 1s under the exact same experimental conditions (same setting parameter of energy analyzer and same mixture of gases and sample temperature). All spectra are calibrated to their corresponding Au 4f_{7/2} which is 84.0 eV. Analyses of XPS peaks are performed with Casa program. Background subtraction influences the accuracy of the calculation of the peak area. For Co 2p (or O 1s) collected at different pressure or temperature, the same parameters including energy window, subtraction of background, line shape, and width are implemented to them, which makes comparison of O/Co ratio measurement at different temperatures valid.

Kinetics studies were performed in a fixed-bed flow reactor. Sample heating is well controlled by a PID controller. The flow rate of each gas was precisely controlled through their own flow meters. Water was introduced through a syringe pump with a precise control of flow rate (3.68 μL min⁻¹). The introduced water was heated to 110 °C and delivered to the catalytic reactor through 10% CO/Ar (aluminum cylinder, Airgas). The ratio of CO to H₂O partial pressures is controlled through the flow rate of liquid water.

Surface chemistry characterization of catalysts during pretreatment or catalysis in Torr pressure range was performed on the in-house AP-XPS daily available in the Tao group.^{40–42} Unlike in vacuum studies, reactant gases are introduced to flow through the catalyst at a certain temperature in the catalysis reactor of AP-XPS while data acquisition is going on. Gas flows through the reactor and exits through the exit port and an aperture that interfaces the gaseous environment in the catalytic reactor and vacuum environment of the pre-lens. Flow rate in the reactor was measured through a mass flow meter installed between each gas source and the entrance of the flow reaction cell. In this study, the flow rate of pure gas is in the range of 3–5 mL pure gas per minute (mL min⁻¹). The total pressure of the mixture gas of reactor is measured with a capacitance gauge installed at the entrance. The pressure at the exit is measured with another capacitance gauge. An average of the pressures at entrance and exit is defined to be the pressure above the catalyst in the catalytic reactor that was integrated with a monochromated Al K α X-ray source and a differential pumping stage. The catalyst is heated through heating the vacuum side of a sample stage using an e-beam heater installed in the vacuum section between the external wall of the catalytic reactor and the internal wall of the UHV chamber. The gaseous side is the internal wall of the reactor. The details are provided in ref 43.

In situ X-ray absorption spectroscopy measurements were performed at the beamline X19A at the National Synchrotron Light Source, Brookhaven National Laboratory. The storage ring energy was 2.5 GeV, and the ring current was in the range of 110–300 mA. A double-crystal Si (111) monochromator was used to scan X-ray energy between 150 eV below and 583 eV above the Pt L_2 edge energy (13270 eV). Both L_3 and L_2 edges are appropriate for probing the d-electron density of Pt, directly affected by electronic charge transfer during the reaction. However, the L_3 edge is much closer in energy to the Co K-edge absorption edge. Hence, the total absorption is relatively high. Therefore, we collected the data at the Pt L_2 edge, which is further away from the Co K-edge energy during catalysis. The energy range was constrained by the onset of the Pt L_1 edge, but the resultant k-range available ($0\text{--}12.1 \text{ \AA}^{-1}$) was sufficiently large for quantitative EXAFS analysis. The samples were made by pressing the powders into circular pellets using a hydraulic press and then transferring them onto the sample holder of a Nashner–Adler in situ cell.^{44,45} The X-ray absorption coefficient in metal Pt foil was measured in the reference mode for X-ray energy calibration and data alignment. Up to five consecutive scans were collected at each stage of the reaction to improve the signal-to-noise ratio.

EXAFS data processing and analysis were performed using the IFEFFIT package. EXAFS data modeling and analysis were performed using standard procedures.^{46,47} The passive electron reduction factor was obtained to be 0.90 ± 0.08 from the fit to the Pt foil data and fixed to be 0.90 in the analysis of all Pt of Pt/Co₃O₄. Several parameters describing electronic properties, specifically, the correction to the original photoelectron energy, and local structural environment (coordination number (N), bond length (R), and mean squared disorder parameter (σ^2) of the nearest neighbors) around absorbing atoms were varied in the fit. Several models were compared for quantitative analysis of the EXAFS data. Theoretical EXAFS signals for Pt–O, Pt–Co, and Pt–Pt contributions were constructed using FEFF6 theory.

3. RESULTS AND DISCUSSION

3.1. WGS on Nominal Catalyst Co₃O₄. Figure 1 presents TEM images of pure cobalt oxide catalyst. The as-synthesized

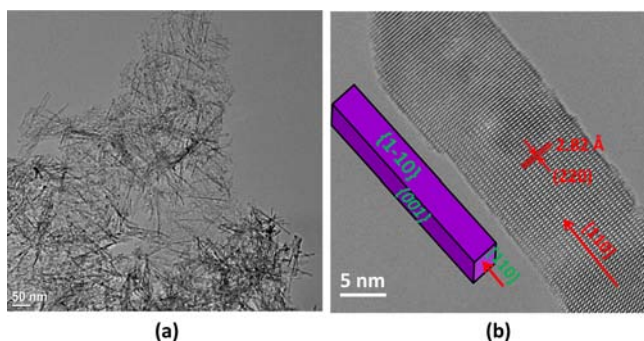


Figure 1. TEM image of Co₃O₄ nanorod catalyst. (a) Large scale. (b) High resolution TEM image.

Co₃O₄ exhibits a rod shape with a size of $\sim 6 \times \sim 6 \times 100\text{--}200$ nm. The measured interplanar distance is 2.82 Å along the extension direction of a nanorod (Figure 1b). Thus, the preferential exposed planes are (1–10) and (001). The two ends of a nanorod are (110). On (001) face, there is only Co³⁺. There are two types of terminal faces (A and B) for (1–10). All Co atoms on the B-type surface are Co³⁺, while Co²⁺ and Co³⁺ coexist on the type A surface of (1–10).

Kinetics studies of WGS on pure Co₃O₄ nanorods experienced a pretreatment at 200 °C in 5% H₂/Ar for 1 h were performed in a micro fixed-bed flow reactor with a flow rate of 150 mL min⁻¹ of mixture of reactants consisting of 3.3%

CO and 3.3% H₂O. The temperature range of the kinetics studies was 180–240 °C. The highest conversion in this temperature regime was controlled to be lower than 15%. An Arrhenius plot (Figure 2) shows that the activation energy of WGS on pure cobalt oxide is $91.0 \pm 10.5 \text{ kJ mol}^{-1}$.

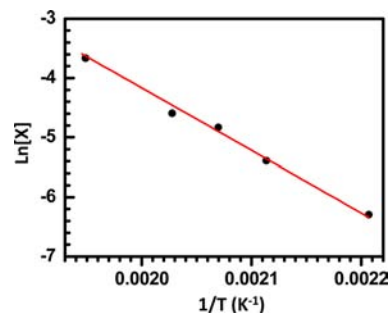


Figure 2. Kinetic studies of WGS on pure Co₃O₄ nanorod catalyst in the temperature range of 180–240 °C.

The surface chemistry of catalyst Co₃O₄ with pretreatment in 5% H₂/Ar at 200 °C and Co₃O₄ without any pretreatment during catalysis was examined using our in-house AP-XPS in the Torr pressure range of a gas mixture of pure CO and pure H₂O. Compared to the partial pressure of H₂O in the mixture of reactants in a micro fixed-bed flow reactor of kinetic studies, ~ 25 Torr, the pressure of the reactant gases in a catalytic reactor of the AP-XPS system, a few Torr, is relatively low. The pressure of reactants contributes to the entropy and Gibbs free energy of the catalyst system, from a thermodynamic point of view. The pressure factor in Gibbs free energy is $kT \times \log P$. A difference in pressure of one magnitude results in a difference of only 0.03 eV in Gibbs free energy.⁴⁸ Typically, such a difference does not lead to an obvious difference in surface chemistry. Thus, we assume that the surface chemistry of the catalyst in a few Torr of reactant gases is almost the same as that in a few tens of Torr of reactant gases, although there could be a large difference between surface chemistry at a few Torr and that in UHV (10^{-10} Torr).⁴⁸

Figure 3 shows the Co 2p and O 1s photoemission feature of Co₃O₄ nanorods, during pretreatment in H₂ at 200 °C, and during the followed catalysis with a flowing mixture of CO and H₂O in the temperature range of 110–300 °C in an AP-XPS reactor. Co 2p_{3/2} and Co 2p_{1/2} of Co₃O₄ at room temperature appear at 779.7 and 794.7 eV, consistent with the data reported

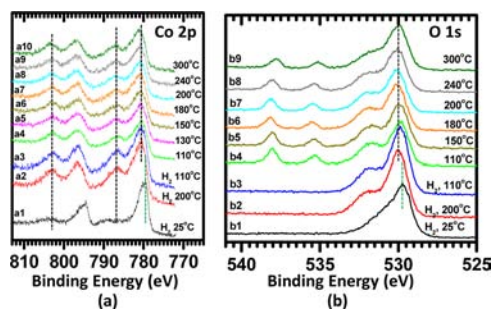


Figure 3. In situ AP-XPS studies of pure cobalt oxide catalyst in pretreatment of H₂ and the following catalysis in the temperature range of 110–300 °C in a mixture of CO and H₂O. The partial pressure ratio is 3:1. All spectra were collected when the gaseous environment existed around the catalyst.

in the literature.^{36,49} However, the photoemission features of both Co 2p and O 1s experience significant change upon Co_3O_4 pretreatment in H_2 at 200 °C; two very clear satellite peaks at 786.5 and 803.0 eV appeared after this pretreatment. The satellite photoemission features at 786.5 and 803.0 eV are characteristic features of Co^{2+} and CoO since only Co^{2+} ions on octahedral sites of rocksalt CoO could result in these unique photoemission features. Co_3O_4 does not have Co^{2+} ions on its octahedral sites. Thus, the observation of satellite peaks at 786.5 and 803.0 eV (Figure 3a) clearly showed a phase transformation from Co_3O_4 to CoO. In addition, the main peaks of Co 2p_{3/2} and Co 2p_{1/2} in CoO upshift by 0.8 eV in contrast to Co_3O_4 . This shift is due to the change of coordination environment of Co ions from Co_3O_4 to CoO. It is another evidence of the phase change during H_2 pretreated at 200 °C (Figure 3a2).

Upon pretreatment, the reactant gases were switched to a mixture of reactants CO and H_2O (Figure 3, parts a3–a10). Photoemission features were collected while the catalyst functioned for WGS. The generation of products during data acquisition of AP-XPS was qualitatively analyzed with a quadrupole mass spectrometer installed at lens 1 of the differential pumping system of AP-XPS.⁴⁰ It performs as real-time analysis of the gas leaking from the catalysis reactor of AP-XPS through the aperture on the catalytic reactor during catalysis. Interestingly, the CoO surface phase remains chemically stable in the mixture of CO and H_2O even at a reaction temperature as low as 110 °C (Figure 3a4). In fact, a photoemission feature of Co 2p of CoO always remained throughout the entire temperature range of WGS, 110–300 °C upon H_2 pretreatment. O 1s photoemission features are presented in Figure 3b. Photoemission features of O 1s from oxygen atoms of gas phases of H_2O and CO were clearly observed at ~536 and ~538 eV, respectively (Figure 3, parts b4–b9). They result from ionization of electrons on the subshell of oxygen atoms of gaseous molecules, which typically give a peak a few eV higher than that of the same subshell from atoms adsorbed on a catalyst surface.^{48,50} It is noted that the observation of photoemission from molecules in the gas phase does not divert assignment of photoemission peaks of molecules adsorbed on the catalyst surface, due to the difference of a few eV in general. Alternatively, it provides solid evidence for the existence of gaseous reactants around the catalyst during data acquisition. Furthermore, the XPS spectra with gas phase peaks can be used to identify product molecules⁵¹ if the conversion in catalytic reactor is high.

Quantitative analysis of photoemission features of Co 2p and O 1s allows us to calculate the O/Co atomic ratio of the surface region of catalysts (Figure 4). Although both CO and H_2O of gas phases around the catalyst contribute to the O 1s photoemission, only O 1s photoemission intensity from surface of cobalt oxide (527–534 eV) was included in the calculation of O/Co atomic ratios. In addition, we assumed an O/Co ratio of Co_3O_4 at room temperature to be 1.33. It is understandable that there are oxygen vacancies on Co_3O_4 surface in a high temperature calcination during preparation. As H_2O molecules in an ambient environment can dissociate on oxygen vacancies and thus OH groups are adsorbed at or fill these oxygen vacancies, the total number of oxygen atoms in the surface region of a Co_3O_4 with adsorbed OH groups at room temperature is approximately close to that of Co_3O_4 without oxygen vacancies. Thus, the O/Co ratio of Co_3O_4 before H_2 pretreatment can be considered to be 1.33. Upon this

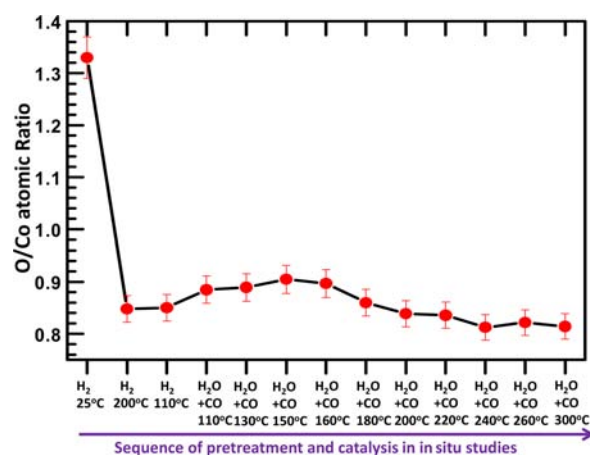


Figure 4. O/Co ratios measured during pretreatment and the following catalysis as a function of the sequential H_2 pretreatment and catalysis. The O/Co ratio of as-synthesized cobalt oxide (Co_3O_4) was defined to be 1.33 which was used to calculate the O/Co ratios at other catalytic conditions.

assumption, a factor can be calculated by dividing the ratio of O 1s to Co 2p peak area with the stoichiometric ratio, 1.33. The atomic ratio of O/Co in pretreatment or during catalysis can be calculated by dividing the area ratio of O 1s to Co 2p at a catalytic condition with this factor calculated above. Figure 4 presents the O/Co atomic ratio as a function of pretreatment or catalytic conditions. Obviously, the O/Co atomic ratio is lower than 1 in H_2 pretreatment at 200 °C and during the following WGS catalysis in 110–300 °C. It shows a reduction of Co_3O_4 to CoO at 200 °C in H_2 . The significant decrease of O/Co ratio is due to the change of surface phase from Co_3O_4 to CoO evidenced by the characteristic satellite peak of Co^{2+} on octahedral sites of CoO (Figure 3). The O/Co ratio remains at ~0.80–0.82 even during catalysis up to 300 °C. The in situ photoemission features of catalysts acquired during catalysis and the measured O/Co ratios in surface region clearly showed that the active phase of nominal catalyst Co_3O_4 nanorods is in fact nonstoichiometric cobalt monoxide, CoO_{1-x} . The easy formation of oxygen vacancies on CoO_{1-x} could result from a larger Co–O bond length³⁷ and relatively weak bond strength in rocksalt CoO, in contrast to those of Co_3O_4 .³⁵

The as-synthesized Co_3O_4 without pretreatment in H_2 was studied by using AP-XPS during catalysis. Figure 5 shows the Co2p and O1s photoemission features at different catalysis temperature. Although cobalt oxide remains in its phase of Co_3O_4 at 100–140 °C in a mixture of reactant CO and H_2O , it is reduced to CoO_{1-x} at 140–160 °C. This is evidenced by the

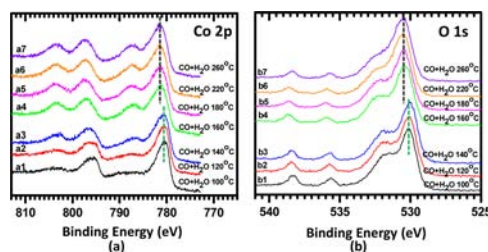


Figure 5. In situ AP-XPS studies of pure cobalt oxide catalyst during catalysis (there is no H_2 pretreatment) in the temperature range of 110–300 °C. The partial pressure ratio is 3:1. All spectra were collected when a catalyst is in a gaseous environment.

appearance of satellite peaks in Figure 5, parts a4–a7. The formation of CoO_{1-x} is also supported by the measured O/Co ratio at a temperature of 140–160 °C. As shown in Figure 6,

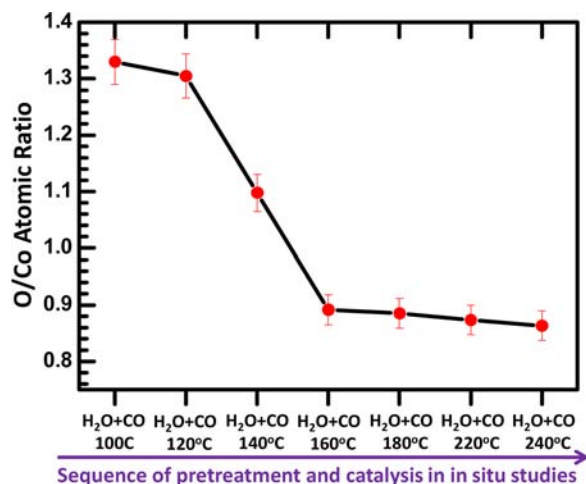


Figure 6. O/Co ratios of pure cobalt oxide catalyst measured during catalysis at different temperature (without H_2 pretreatment).

when temperature is higher than 140 °C, the O/Co ratio is decreased to 0.88 or so. Obviously, the surface phase during catalysis in temperature regime of 160–300 °C is CoO_{1-x} which is the same as that of Co_3O_4 first pretreated in H_2 at 200 °C (Figures 3 and 4). Kinetics studies of Co_3O_4 (without pretreatment in H_2) in the temperature range of 180–240 °C show that its activation energy is very close to 91.0 kJ mol^{-1} of the catalyst experienced a pretreatment in H_2 (Figure 2). The same surface chemistry and almost identical activation energy for catalyst *with a H_2 pretreatment* and *without a H_2 pretreatment* suggested that the active phase CoO_{1-x} can be formed in a mixture of reactant gases ($\text{CO} + \text{H}_2\text{O}$) and products ($\text{H}_2 + \text{CO}_2$) during catalysis at certain reaction temperature even though there is no any H_2 pretreatment before WGS reaction.

The phase transformation of the Co_3O_4 catalyst under reaction conditions was studied with environmental TEM. As shown in Figure 7a, the bulk phase of Co_3O_4 in 0.3 Torr of reactant gases is transformed to CoO at 300 °C or so. In addition, the first peak of the O–K edge of Co_3O_4 (Figure 7d) observed at 200 °C disappears when the catalyst in the reactant gases was heated to 300 °C. The O–K edge resulting from the

reactant gas was subtracted from the EELS spectra. The O–K edge starts to be weakened at 200 °C and disappears at 300 °C (Figure 7d). The EELS spectrum of the CoO in the reactant gases at 300 °C is consistent with the previous EELS spectrum of CoO under high vacuum.^{52–54}

In summary, pure Co_3O_4 is restructured to nonstoichiometric CoO_{1-x} in the reactants (CO and H_2O) of WGS. This was confirmed in our in situ studies of AP-XPS and E-TEM. CoO_{1-x} is active for WGS, with an activation energy of $91.0 \pm 10.5 \text{ kJ mol}^{-1}$ in the temperature range of 180–240 °C.

3.2. WGS on Cobalt Oxide Anchoring Pt Atoms. Pt/ Co_3O_4 was synthesized through two steps. The first step is the synthesis of Co_3O_4 nanorods. After it is synthesized, Pt ions are anchored through deposition–precipitation, followed by a mild drying process and a subsequent calcination at 250 °C. TEM studies showed that the surface morphology is basically preserved, although roughening of the edge of the Co_3O_4 nanorods to some extent was definitely identified. The weight ratio of Pt to Co_3O_4 is 0.5%, equivalent to a Pt/Co atomic ratio of 0.2%. Since Pt ions were anchored on the surface of precrystallized Co_3O_4 nanorods through calcination at 250 °C, Pt ions are anchored on surface of Co_3O_4 nanorods. The atomic ratio (2.4%) of Pt to Co on the surface of a nanorod is actually much larger than the overall ratio (0.2%), since Pt atoms are anchored on Co_3O_4 already well crystallized. Calculations show that the low concentration of Pt atoms on a surface, $\text{Pt}_{\text{surface}}/\text{Co}_{\text{surface}} = 2.4\%$ (see Supporting Information) certainly prevents them from aggregating to form Pt nanoclusters. STEM of the as-synthesized Pt/ Co_3O_4 shows that the majority of Pt atoms are singly dispersed (Figure 8). This identification is consistent with the measured coordination number of Pt to Pt, zero, through analysis of EXAFS data of this catalyst to be described later in this work. As the Pt atom does not bond with another Pt atom in the as-synthesized 0.2% Pt/ Co_3O_4 , we call this as-synthesized catalyst, Co_3O_4 anchoring singly dispersed Pt atoms. It is written as $\text{Pt}_1/\text{Co}_3\text{O}_4$. In fact, EXAFS studies showed these Pt atoms in the as-synthesized catalyst bond solely to O atoms instead of Co.

Catalysis studies of Pt/ Co_3O_4 were performed in a micro flow reactor. Kinetics measurements were performed in a kinetic control regime. Figure 9 is the Arrhenius plot in a temperature regime of 150–200 °C. On the basis of this plot activation energy of the catalyst is $50.1 \pm 5.0 \text{ kJ mol}^{-1}$, much lower than the $91.0 \pm 10.5 \text{ kJ mol}^{-1}$ of CoO_{1-x} (Figure 2). More interestingly, kinetic measurement in the temperature

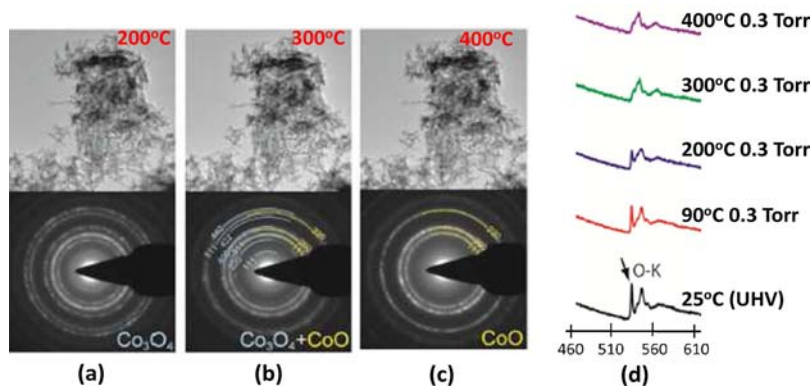


Figure 7. In situ TEM studies of Co_3O_4 nanorod catalysts at 0.3 Torr of reactant gas. (a)–(c): In situ diffraction patterns of Co_3O_4 nanorods in 0.3 Torr reactant gases at 200 °C, 300 °C, and 400 °C. (d) EELS spectra of Co_3O_4 nanorods at different temperatures in 0.3 Torr reactants.

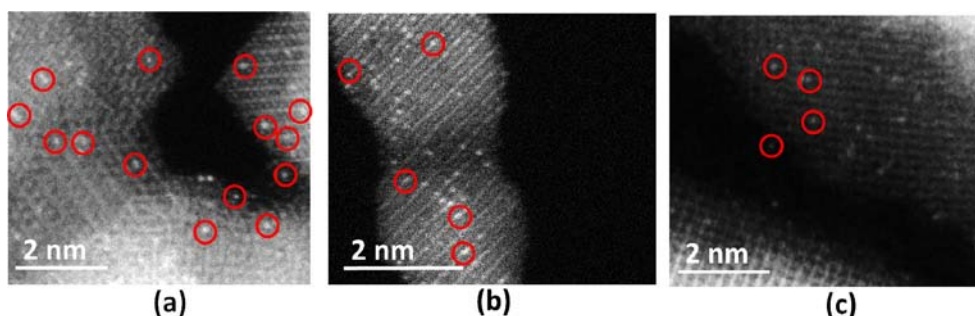


Figure 8. Images of aberration-corrected annular dark-field scanning transmission electron microscopy studies of Co_3O_4 with singly dispersed Pt atoms, $\text{Pt}_1/\text{Co}_3\text{O}_4$. Spots with high contrast (marked with red circles) are Pt atoms singly dispersed on Co_3O_4 nanorods. Images (a), (b), and (c) were collected at different areas randomly selected.

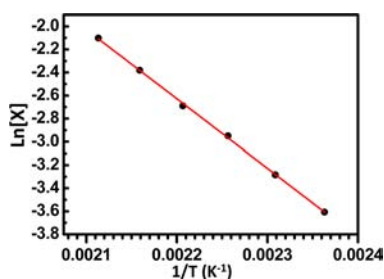


Figure 9. Kinetics studies of WGS on $\text{Pt}_1\text{Co}_x/\text{Co}_3\text{O}_4$ catalyst in the temperature range of 180–240 °C.

range of 300–350 °C exhibits quite different kinetics, as shown in Figure 10a. The activation energy in 300–350 °C is $24.8 \pm 3.1 \text{ kJ mol}^{-1}$. The two quite different activation energies suggest different active phases in these two temperature ranges (150–200 °C versus 300–350 °C).

Figure 11 shows the photoemission features of Co 2p and Pt 4d_{5/2} of $\text{Pt}_1/\text{Co}_3\text{O}_4$ at room temperature and during catalysis at 150 °C, 200 °C, 280 °C, and 350 °C. Obviously, Co 2p remains the photoemission feature of Co_3O_4 at room temperature (Figure 11a1) and during catalysis at 150–200 °C (Figure 11, parts a2 and a3) since there are no any characteristic satellite peaks of Co^{2+} of rocksalt CoO at 786.5 and 803.0 eV. The preservation of Co_3O_4 phase up to 200 °C during catalysis was further supported by the O/Co ratio of 1.10–1.15 at 150–200 °C. If the surface phase were CoO_{1-x} , then the O/Co ratio should have been 1 or lower. Thus, there is no phase transformation from Co_3O_4 to CoO in $\text{Pt}/\text{Co}_3\text{O}_4$ catalyst in the temperature range of 150–200 °C.

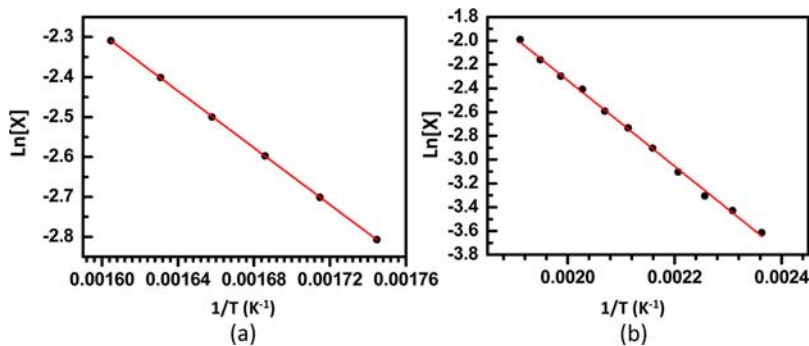


Figure 10. Kinetic studies of WGS on $\text{Pt}_m\text{Co}_m/\text{CoO}_{1-x}$ catalyst in the temperature range of 300–350 °C (a) and 140–240 °C upon cooling it from 350 °C to 140 °C (b).

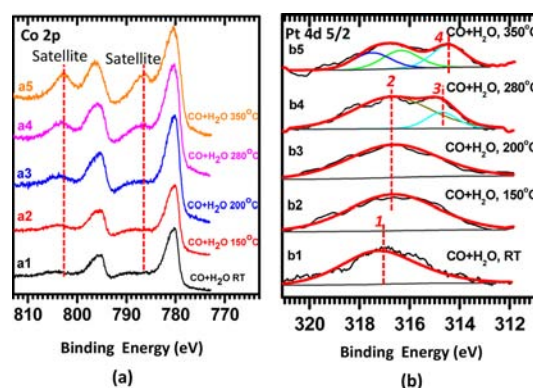


Figure 11. Photoemission features of Co 2p and Pt 4d_{5/2} of as-synthesized $\text{Pt}_1/\text{Co}_3\text{O}_4$ catalyst during catalysis at different temperatures. (a) Co 2p and (b) Pt 4d_{5/2}. As Pt 4f overlaps photoemission features of Co 3p, Pt 4d_{5/2} was used to identify oxidation state and chemical environment of Pt anchored on Co_3O_4 .

EXAFS studies were performed during catalysis in the temperature range of 25–300 °C. Figure 12 presents the Fourier transformed EXAFS data collected at the Pt L₂ edge at 25 and 200 °C during catalysis and their fitting analyses. Details of the fitting were described in the Experimental Section. The data and theoretical fit of metallic Pt are shown in Figure 12b. Figure 12c presents the fitting for data of the as-synthesized $\text{Pt}-\text{Co}_3\text{O}_4$ catalyst. This fitting suggests that Pt bonds predominantly with oxygen atoms instead of any Co atoms or Pt atoms. The measured coordination number of O atoms to a Pt atom is about 4.1 ± 1.9 (Table 1).

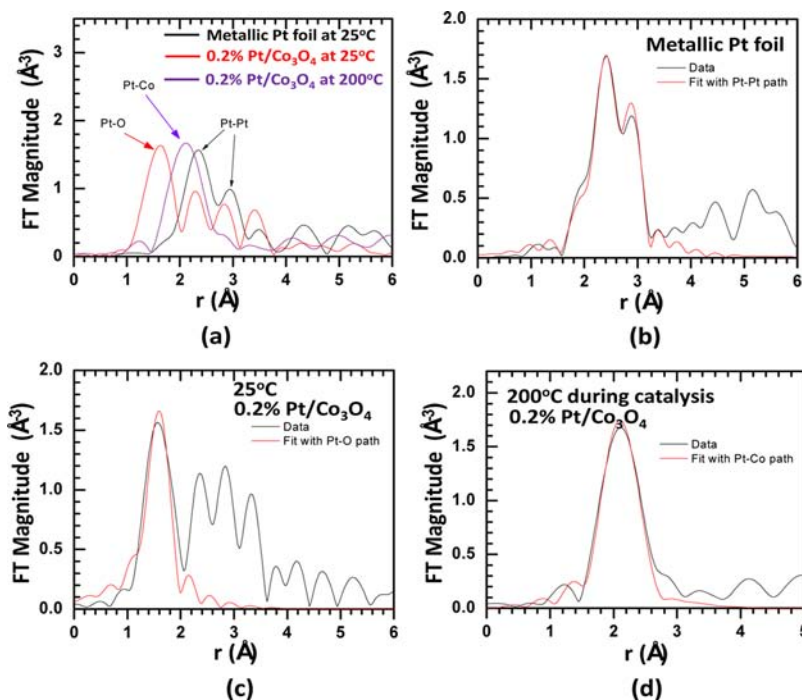


Figure 12. Catalytic in situ Pt L_2 -edge EXAFS data and theoretical fits of Pt_1/Co_3O_4 at 25 °C and during catalysis at 200 °C. For comparison, data of metallic Pt foil were included as well. (a) Experimental data collected. (b) Fitting with Pt–Pt path of metallic Pt foil. (c) Fitting with Pt–O bond of as-synthesized Pt_1/Co_3O_4 at 25 °C. (d) Fitting with Pt–Co path of Pt_1/Co_3O_4 at 200 °C during catalysis.

Table 1. Results of Quantitative Analyses for Pt–Pt, Pt–O, and Pt–Co Contributions to the EXAFS Data Obtained at 25 °C and during WGS at 200 °C^a

sample	N(Pt–O)	N(Pt–Co)	R(Pt–O), Å	R(Pt–Co), Å
25 °C, as prepared	4.1 ± 1.9	0	2.01 ± 0.04	
200 °C, during WGS reaction	0	7.1 ± 1.5		2.54 ± 0.01

^aResults of metallic Pt foil are shown as well for comparison. Only the coordination numbers and pair distances are shown. Standard deviations in the distances are shown in the SI.

EXAFS data at 200 °C during catalysis (Figure 12d) show that there is no presence of Pt–Pt or Pt–O bonds and the data are dominated by Pt–Co bonds. The quantitative analyses show that the coordination number of Co to Pt is 7.1 ± 1.5 (Table 1). The data indicate that Pt forms singly dispersed $PtCo_n$ nanoclusters on the oxide substrate during catalysis at 200 °C. Thus, the as-synthesized catalyst restructures to a new surface phase, Pt_1Co_n ($n = 7.1 \pm 1.5$)/ Co_3O_4 in which Pt_1Co_n ($n = 7.1 \pm 1.5$) is singly distributed on Co_3O_4 surface.

Although the analysis of EXAFS data collected during catalysis at 200 °C demonstrate that Pt–Co dominates the experimental spectrum, such evidence is lacking for the catalyst during catalysis at 250 and 300 °C. Quantitative EXAFS analysis is not possible for the data of 250 and 300 °C due to the decreasing amplitude of EXAFS oscillations at these high temperature and, as a result, the poor signal-to-noise ratio. To examine the behavior of the catalyst at these high temperatures, 250 and 300 °C, we examined the X-ray absorption near edge structure (XANES) during catalysis at these temperatures, which is less affected by the catalysis temperature than the EXAFS data. Figure S6 of the SI presents the distinctive difference in the three regions (A, B, C) between XANES data at 200 °C corresponding to Pt_1Co_n/Co_3O_4 (Phase I) and those

at 250 and 300 °C attributable to $Pt_mCo_{m'}/CoO_{1-x}$ (Phase II). The spectra at 250 and 300 °C (blue and yellow curves in Figure S6 of the SI) behave similarly to the metallic Pt foil (black curve in Figure S6 of the SI), while the spectrum at 200 °C (red curve in Figure S6 of the SI) shows distinct differences in these regions. This similarity of the XANES spectra during catalysis at 250 and 300 °C with Pt foil (black curve in Figure S8 of the SI) suggests that the sample at 250 and 300 °C contains Pt–Pt bonding contributions, in addition to Pt–Co.

The restructuring revealed in EXAFS studies is further supported by the AP-XPS data (Figure 11). To avoid overlap of Pt 4f with tail of Co 3p photoemission feature, Pt 4d_{5/2} was used to identify chemical state of Pt atoms during catalysis. The photoemission feature of Pt 4d_{5/2} has a wider distribution in terms of its full width at half-maximum (fwhm) due to its intrinsic short core-hole lifetime. The peak position of Pt 4d_{5/2} of the as-synthesized Pt_1/Co_3O_4 is 317.1 eV, which is consistent with Pt 4d_{5/2} of platinum oxide.^{55,56} At 150 °C, the peak is broadened and down shifted by 0.7 to 316.4 eV during catalysis at 150 °C and remains the same photoemission feature at 200 °C during catalysis (Figure 11, parts b2 and b3). This down-shift results from a switch of binding environment of Pt atoms from Pt–O to Pt–Co based on EXAFS studies. Notably, the peak position of Pt 4d_{5/2} of $PtCo_n$ is still about 2 eV higher than metallic Pt,⁵⁵ resulting from the fact that each of the neighboring Co atoms of a Pt atom bonds with a few oxygen atoms (Figure 13b). This bonding likely makes Pt still positively charged to some extent. Thus, it still exhibits a binding energy higher than metallic Pt (Figure 11, parts b2 and b3).

These in situ studies showed that the active phase at 150–200 °C is Pt_1Co_n nanoclusters embedded in the top layer of Co_3O_4 . Figure 13, parts a and b, presents the structure of Co_3O_4 anchoring singly distributed $PtCo_n$ nanoclusters. The activation energy in the temperature range of 150–200 °C is

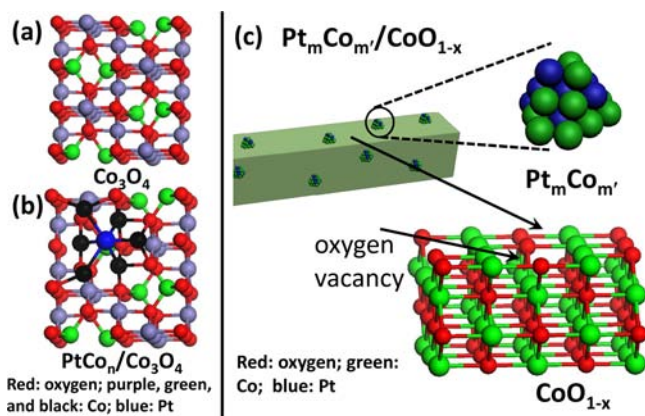


Figure 13. Structural models of surfaces of pure Co_3O_4 and active catalysts. (a) Top view of pure Co_3O_4 . (b) Top view of $\text{Pt}_1\text{Co}_n/\text{Co}_3\text{O}_4$. (c) $\text{Pt}_m\text{Co}_{m'}/\text{CoO}_{1-x}$.

$\sim 50.1 \pm 5.0 \text{ kJ mol}^{-1}$ (Figure 9). The TOF of $\text{Pt}_1\text{Co}_n/\text{Co}_3\text{O}_4$ at 200°C based on the conversion measured in kinetics control regime is 0.40 H_2 molecules per Pt site per second. $\text{Pt}_1\text{Co}_n/\text{Co}_3\text{O}_4$ at 200°C is ten times more active than Pt/CeO_2 at this temperature. This TOF (200°C) is approximately equal to or higher than that of Pt/CeO_2 at 300°C (Table 2, Figure 14). In addition, $\text{Pt}_1\text{Co}_n/\text{Co}_3\text{O}_4$ exhibits a high catalytic activity at 150°C (TOF = 0.089). It suggests a very good catalytic performance of $\text{Pt}_1\text{Co}_n/\text{Co}_3\text{O}_4$ at low temperature such as 150°C , although Pt/CeO_2 at 150°C is not active. $\text{Pt}_m\text{Co}_{m'}/\text{CoO}_{1-x}$ formed through restructuring $\text{Pt}_1\text{Co}_n/\text{Co}_3\text{O}_4$ exhibits much higher TOF, 0.27 and 0.58 H_2 molecules per Pt site per second at 150 and 200°C , respectively (Table 2), due to its low activation barrier of 29.6 kJ/mol .

As seen in Figure 11, parts a3–a5, the AP-XPS studies clearly showed a phase transition of Co_3O_4 of $\text{Pt}_1\text{Co}_n/\text{Co}_3\text{O}_4$ to CoO_{1-x} in the temperature range of $200\text{--}300^\circ\text{C}$. The main evidence is the appearance of a pair of satellite peaks of Co 2p of Co^{2+} on the octahedral site of the oxygen atoms (Figure 11a5). The satellite peaks of Co 2p at 300°C (Figure 11a5) are obvious. In addition, the O/Co ratio of catalysts at 300°C is ~ 0.80 (not shown), further supporting a phase transformation from Co_3O_4 to CoO_{1-x} in the temperature range of $250\text{--}300^\circ\text{C}$.

The change at a temperature of 280°C reflects the chemical state of the Pt ions. An additional photoemission of the Pd 4d5/2 feature of the doped catalyst at a temperature of 280°C (Figure 11b4) exhibits a broad peak centered at a low binding energy at $\sim 315.8 \text{ eV}$. It showed an obvious change in the chemical states of the Pt atoms in the temperature range of $250\text{--}300^\circ\text{C}$. Since Co_3O_4 of the catalyst is reduced to $\text{CoO}_{0.8}$ in the temperature range of $200\text{--}300^\circ\text{C}$ (Figure 11, parts a3–a5), we would consider that new Pt–Co nanoclusters are formed in the phase transformation from Co_3O_4 to CoO . The binding energy of Pt 4d5/2 at 280°C (peak 2) is obviously down-shifted by 0.5 eV in contrast to peak 1 at room temperature. Notably, an obvious low-energy shoulder at 314.4 eV (peaks 3 and 4 in Figure 11, parts b4 and b5, respectively) appeared at 280 and 350°C in contrast to those of 200°C in the first annealing cycle (Figure 11b3). The position of the low-energy shoulder is consistent with the Pt 4d5/2 of Pt metal found in the literature.^{64,65} Since the contribution from metallic Pt at 314.4 eV was clearly identified and there is still a large contribution at 316.4 eV attributable to Pt–Co, we would

Table 2. List of Turnover-Frequency of Catalysts Reported in This Work and Pt–CeO₂ and Pt–TiO₂ in the Literature

temperature ($^\circ\text{C}$)	Pt _m Co _m /CoO _{1-x}			Pt/CeO ₂		Pt/TiO ₂	
	CoO _{1-x}	Pt ₁ Co _n /Co ₃ O ₄	Pt _m Co _m /CoO _{1-x}	0.052 (ref 57)	0.037 (ref 58)	0.093 (ref 57)	0.093 (ref 58)
150		0.089	0.27 ^a	0.44 (ref 57)	0.21 (ref 58)	0.50 (ref 57)	0.28 (ref 58)
200	0.000261	0.40	0.58 ^a		0.08 (ref 58)		0.37 (ref 58)
250	0.00147		0.84 ^a		0.27 (ref 58)		
300			2.37 ^a	0.39 (ref 58)			
350			3.90 ^a				

^aTOF of $\text{Pt}_m\text{Co}_m/\text{CoO}_{1-x}$ when all Pt atoms are assumed to be active sites.

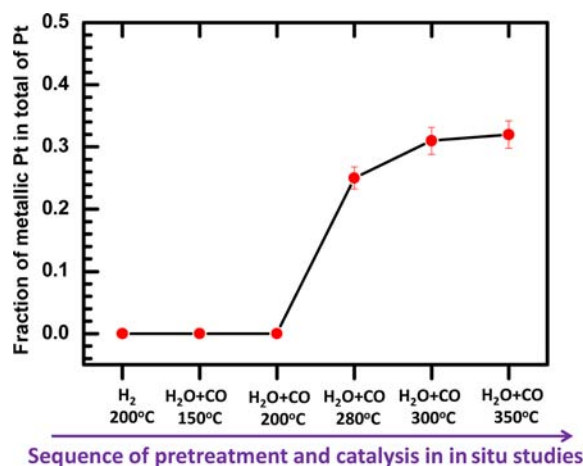


Figure 14. Atomic fraction of Pt of Pt 3d peak with a binding energy at 314.2 eV based on a consistent deconvolution of Pt 3d photoemission features of nominal catalyst Pt/Co₃O₄ during catalysis. The active phases of the catalysts in the temperature range of 150–200 °C and 300–350 °C are PtCo_m/Co₃O₄ and Pt_mCo_m/CoO_{1-x} respectively.

suggest that bimetallic nanoclusters Pt_mCo_m were formed along the restructuring of Co₃O₄ substrate to CoO_{1-x} in the mixture of reactant gases. Our in situ AP-XPS studies and the deconvolution of spectra of Pt_mCo_m/CoO_{1-x} obtained at 350 °C (Figure 11b5) showed that the Pt 4d5/2 photoemission feature of Pt_mCo_m/CoO_{1-x} is contributed from Pt–O at 317.5 eV,⁵⁶ Pt–Co–O at 316.4 eV, and Pt–Pt at 314.4 eV,⁵⁵ respectively. The three features contribute ~36%, ~32%, and ~32% of the intensity of Pt 4d5/2, respectively (Figure 11b5). From these analyses, approximately 32% of atoms of a Pt_mCo_m nanocluster are Co atoms, on average.

In each of such Pt_mCo_m nanoclusters, some Pt atoms bond with Pt atoms and the other with Co and O atoms. As Co₃O₄ is reduced to CoO_{1-x} at 300 °C, we would term the active phase to be Pt_mCo_m/CoO_{1-x}. Figure 13c presents the structural scheme of Pt_mCo_m/CoO_{1-x}. Compared to pure CoO_{1-x} formed from pure Co₃O₄ (Figure 2), the activation energy on Pt_mCo_m/CoO_{1-x} (Figure 10) is much lower, which clearly suggests the significance of Pt_mCo_m nanoclusters (Table 3).

Table 3. Activation Energies of Co₃O₄ (Nominal Catalyst) and Pt₁/Co₃O₄ (Nominal Catalyst), and Pt/CeO₂ and Pt/TiO₂

nominal catalyst	surface of active catalyst	activation energy (kJ/mol)	temperature range of kinetic studies (°C)	references
Co ₃ O ₄	CoO _{1-x}	91.0	180–280	this work
0.2%Pt/Co ₃ O ₄	PtCo _n /Co ₃ O ₄	49.9	150–200	this work
0.2%Pt/Co ₃ O ₄	Pt _m Co _m /CoO _{1-x}	24.8	300–350	this work
		29.6	140–240	this work
Pt–CeO ₂	Pt/CeO _{2-x}	46.1	150–350	ref 61
		91 ± 5	150–400	ref 60
		100.48	200–250	ref 57
		60 ± 2	175–250	ref 62
		45.2	200–420	ref 59
Pt–TiO ₂	Pt/TiO _{2-x}	45.2	200–420	ref 59
		59 ± 3	150–400	ref 60
		64.9	180–280	ref 57
		65.7	180–280	ref 63

To examine a potential influence of gas composition on kinetic studies and surface chemistry of catalysts, measurement of the E_a of as-synthesized Pt₁/Co₃O₄ catalyst in the two different temperature ranges of 150–200 °C and 300–350 °C were performed in a mixture of reactants CO and H₂O with a ratio of 1:3 instead of the 3:1 ratio used in Figures 9 and 10. In the temperature range of 150–200 °C, the measured E_a of catalysts in the reactions of CO and H₂O, with a ratio of 1:3, is close to the 50.1 ± 5.0 kJ mol⁻¹ value measured in the mixture of CO and H₂O, with a ratio of 3:1. In the temperature range of 300–350 °C, it is 29.6 ± 4.0 kJ mol⁻¹, similar to the 24.8 ± 3.1 kJ mol⁻¹ value found for the CO:H₂O ratio of 3:1. These studies suggest that the gas composition of reactants does not obviously vary the kinetics and surface chemistry of Pt₁Co_n/Co₃O₄ and Pt_mCo_m/CoO_{1-x}.

Table 3 lists the activation energies of CoO_{1-x}, PtCo_n/Co₃O₄, Pt_mCo_m/CoO_{1-x} measured here, and Pt/CeO₂ and Pt/TiO₂ reported in the literature. Pt_mCo_m/CoO_{1-x} has the lowest activation energy. The turnover frequency of generation of H₂ on the three catalysts at different temperatures was calculated. They are listed in Table 2. When compared to the TOF of H₂ generation on Pt/CeO₂ and Pt/TiO₂, Pt_mCo_m/CoO_{1-x} exhibits a higher TOF (Table 2). For example, the TOF at 350 °C Pt_mCo_m/CoO_{1-x} is 35 times higher than that of Pt/TiO₂ at this temperature. Notably, the Pt_mCo_m/CoO_{1-x} phase exhibits a high catalytic activity in the low-temperature range of 140–240 °C, upon being cooled to 140 °C from 350 °C. Figure 10b is the Arrhenius plot in this temperature regime. The activation energy calculated from this Arrhenius plot is 29.6 kJ/mol. It is in good agreement with the activation energy measured at the high temperatures of 300–350 °C. The higher catalytic activity of Pt_mCo_m/CoO_{1-x} in contrast to Pt/CeO₂ is likely partially contributed from both the difference in the metal components (Pt_mCo_m/CoO_{1-x} nanoclusters versus Pt nanoparticles) and the difference in the reducible oxides (nonstoichiometric CoO_{1-x} versus CeO₂). Oxygen vacancies of reducible oxides such as CeO₂ and TiO₂ are considered to be the sites of adsorption with a following dissociation of H₂O.⁷ Similarly, we consider oxygen vacancies of CoO_{1-x} on Pt_mCo_m/CoO_{1-x} to be the sites that disassociate H₂O. Different from oxygen vacancies in CeO₂ and TiO₂, an oxygen vacancy on CoO_{1-x} could retain a pair of electrons. It is similar to an oxygen vacancy of MgO.^{66–68} However, the Ce or Ti atom of an oxygen vacancy on CeO_{2-x} and TiO_{2-x} is in fact in a reduced valence state, Ce³⁺ and Ti³⁺. It seems that an oxygen vacancy on the surface of CoO_{1-x} has a different electronic structure compared to those on CeO_{2-x} and TiO_{2-x}. We expect that oxygen vacancies on the CoO_{1-x} surface play a role similar to that of the MgO surface with regard to adsorption and dissociation of H₂O. Both experimental and theoretical studies have shown that dissociation of H₂O on an MgO surface is performed by oxygen vacancies.^{67,68} Computational studies on the electronic structures of the oxygen vacancies of CoO_{1-x} and its adsorption of H₂O would certainly help in our understanding of the role of CoO_{1-x} in Pt_mCo_m/CoO_{1-x}.

4. CONCLUSIONS

We reported three different WGS catalysts, CoO_{1-x}, Pt₁Co_n/Co₃O₄, and Pt_mCo_m/CoO_{1-x}. Their active surfaces during catalysis were identified with different in situ surface analytical techniques: AP-XPS, EXAFS, and E-TEM. Their kinetics were studied in the kinetic control regime. Pt_mCo_m/CoO_{1-x} exhibits the lowest activation energy in contrast to pure CoO_{1-x} and

Pt₁Co_n/Co₃O₄, probably due to the synergic effect of the nanoclusters Pt_mCo_{m'} and oxygen vacancies of CoO_{1-x}. Oxygen vacancies of CoO_{1-x} could play a different role in the adsorption and dissociation of H₂O molecules in contrast to that of CeO_{2-x} and TiO_{2-x}. The different catalytic performances of CoO_{1-x}, Pt₁Co_n/Co₃O₄, and Pt_mCo_{m'}/CoO_{1-x} restructured from Co₃O₄ and Pt₁/Co₃O₄, suggested a method of tuning catalytic performance and developing catalysts through restructuring the oxide catalyst in the gas phases.

■ ASSOCIATED CONTENT

● Supporting Information

Synthesis of catalysts; calculation of the atomic ratio of Pt to Co atoms on topmost surface of a 0.2% Pt₁/Co₃O₄ nanorod; standard deviation in analysis of Pt–O, Pt–Co, and Pt–Pt bonds from EXAFS data; ambient pressure X-ray photoelectron spectroscopy and in situ studies of surface chemistry of catalysts during catalysis and under reaction conditions; analysis of X-ray absorption near edge structure of catalysts during catalysis; and ADF-STEM images of Pt_mCo_{m'} nanoclusters formed during catalysis at high temperatures. This material is available free of charge via the Internet at <http://pubs.acs.org>.

■ AUTHOR INFORMATION

Corresponding Author

ftao@nd.edu

Author Contributions

[†]These authors contributed equally to this work.

Notes

The authors declare no competing financial interest.

■ ACKNOWLEDGMENTS

This work is supported by the Chemical Sciences, Geosciences and Biosciences Division, Office of Basic Energy Sciences, Office of Science, U.S. Department of Energy under Grant No. DE-FG02-12ER1635. XANES and EXAFS experiments were supported by the Chemical Sciences, Geosciences and Biosciences Division, Office of Basic Energy Sciences, Office of Science, U.S. Department of Energy under the Grant No. DE-FG02-03ER15476 (to A.I.F.). Beamline X18B at the NSLS is supported in part by the Synchrotron Catalysis Consortium, U.S. Department of Energy Grant No. DE-FG02-05ER15688.

■ REFERENCES

- (1) Navarro, R. M.; Pena, M. A.; Fierro, J. L. G. *Chem. Rev.* **2007**, *107*, 3952.
- (2) Babita, K.; Sridhar, S.; Raghavan, K. V. *Int. J. Hydrogen Energy* **2011**, *36*, 6671.
- (3) Park, E. D.; Lee, D.; Lee, H. C. *Catal. Today* **2009**, *139*, 280.
- (4) Tanksale, A.; Beltramini, J. N.; Lu, G. Q. M. *Renew. Sust. Energy Rev.* **2010**, *14*, 166.
- (5) Ratnasamy, C.; Wagner, J. P. *Catal. Rev.* **2009**, *51*, 325.
- (6) Fu, Q.; Saltsburg, H.; Flytzani-Stephanopoulos, M. *Science* **2003**, *301*, 935.
- (7) Rodriguez, J. A.; Ma, S.; Liu, P.; Hrbek, J.; Evans, J.; Perez, M. *Science* **2007**, *318*, 1757.
- (8) Zhai, Y. P.; Pierre, D.; Si, R.; Deng, W. L.; Ferrin, P.; Nilekar, A. U.; Peng, G. W.; Herron, J. A.; Bell, D. C.; Saltsburg, H.; Mavrikakis, M.; Flytzani-Stephanopoulos, M. *Science* **2010**, *329*, 1633.
- (9) Si, R.; Flytzani-Stephanopoulos, M. *Angew. Chem., Int. Ed.* **2008**, *47*, 2884.
- (10) Henrich, V. E.; Cox, P. A. *The Surface Science of Metal Oxides*, 2nd ed.; Cambridge University Press: New York, 2000.

- (11) Vindigni, F.; Manzoli, M.; Damin, A.; Tabakova, T.; Zecchina, A. *Chem.—Eur. J.* **2011**, *17*, 4356.
- (12) Xu, W.; Si, R.; Senanayake, S. D.; Llorca, J.; Idriss, H.; Stacchiola, D.; Hanson, J. C.; Rodriguez, J. A. *J. Catal.* **2012**, *291*, 117.
- (13) Wieder, N. L.; Cargnello, M.; Bakhmutsky, K.; Montini, T.; Fornasiero, P.; Gorte, R. J. *J. Phys. Chem. C* **2011**, *115*, 915.
- (14) Schweitzer, N. M.; Schaidle, J. A.; Ezekoye, O. K.; Pan, X.; Linic, S.; Thompson, L. T. *J. Am. Chem. Soc.* **2011**, *133*, 2378.
- (15) Shekhar, M.; Wang, J.; Lee, W. S.; Williams, W. D.; Kim, S. M.; Stach, E. A.; Miller, J. T.; Delgass, W. N.; Ribeiro, F. H. *J. Am. Chem. Soc.* **2012**, *134*, 4700.
- (16) Williams, W. D.; Shekhar, M.; Lee, W. S.; Kispersky, V.; Delgass, W. N.; Ribeiro, F. H.; Kim, S. M.; Stach, E. A.; Miller, J. T.; Allard, L. F. *J. Am. Chem. Soc.* **2010**, *132*, 14018.
- (17) Goguet, A.; Burch, R.; Y., C.; Hardacre, C.; Hu, P.; Joyner, R. W.; Meunier, F. C.; Mun, B. S.; Thompsett, D.; Tibiletti, D. *J. Phys. Chem. C* **2007**, *111*, 16927.
- (18) Jacobs, G.; Williams, L.; Graham, U.; Sparks, D.; Davis, B. H. *J. Phys. Chem. B* **2003**, *107*, 10398.
- (19) Si, R.; Tao, J.; Evans, J.; Park, J. B.; Barrio, L.; Hanson, J. C.; Zhu, Y.; Hrbek, J.; Rodriguez, J. A. *J. Phys. Chem. C* **2012**, *116*, 23547.
- (20) Han, W.-Q.; Wen, W.; Hanson, J. C.; Teng, X.; Marinkovic, N.; Rodriguez, J. A. *J. Phys. Chem. C* **2009**, *113*, 21949.
- (21) Frenkel, A. I.; Rodriguez, J. A.; Chen, J. G. *ACS Catal.* **2012**, *2*, 2269.
- (22) Rodriguez, J. A.; Liu, R.; Hrbek, J.; Perez, M.; Evans, J. *J. Mol. Catal. A: Chem.* **2008**, *281*, 59.
- (23) Zhao, X.; Ma, S.; Hrbek, J.; Rodriguez, J. A. *Surf. Sci.* **2007**, *601*, 2445.
- (24) Wang, X.; Rodriguez, J. A.; Hanson, J. C.; Perez, M.; Evans, J. *J. Chem. Phys.* **2005**, *123*, 221101.
- (25) Wang, X. Q.; Rodriguez, J. A.; Hanson, J. C.; Gamarra, D.; Martinez-Arias, A.; Fernandez-Garcia, M. *J. Phys. Chem. B* **2006**, *110*, 428.
- (26) Rodriguez, J. A.; Ma, S.; Liu, P.; Hrbek, J.; Evans, J.; Perez, M. *Science* **2007**, *318*, 1757.
- (27) Fu, Q.; Saltsburg, H.; Flytzani-Stephanopoulos, M. *Science* **2003**, *301*, 935.
- (28) Zhai, Y.; Pierre, D.; Si, R.; Deng, W.; Ferrin, P.; Nilekar, A. U.; Peng, G.; Herron, J. A.; Bell, D. C.; Saltsburg, H.; Mavrikakis, M.; Flytzani-Stephanopoulos, M. *Science* **2010**, *329*, 1633.
- (29) Shido, T.; Iwasawa, Y. *J. Catal.* **1993**, *141*, 71.
- (30) Burch, R. *J. Phys. Chem. Chem. Phys.* **2006**, *8*, 5483.
- (31) Xie, X. W.; Li, Y.; Liu, Z. Q.; Haruta, M.; Shen, W. *J. Nature* **2009**, *458*, 746.
- (32) Xie, X. W.; Shang, P. J.; Liu, Z. Q.; Lv, Y. G.; Li, Y.; Shen, W. *J. Phys. Chem. C* **2010**, *114*, 2116.
- (33) Yu, Y.; Takei, T.; Ohashi, H.; He, H.; Zhang, X.; Haruta, M. *J. Catal.* **2009**, *267*, 121.
- (34) Brundle, C. R.; Chuang, T. J.; Rice, D. W. *Surf. Sci.* **1976**, *60*, 286.
- (35) Shantyr, R., Martin-Luther-Universität Halle-Wittenberg, 2004.
- (36) Chuang, T. J.; Brundle, C. R.; Rice, D. W. *Surf. Sci.* **1976**, *59*, 413.
- (37) Gubo, M.; Ebersperger, C.; Meyer, W.; Hammer, L.; Heinz, K. *J. Phys. Condens. Matter* **2009**, *21*, 474211.
- (38) Jiang, D.-e.; Dai, S. *J. Phys. Chem. Chem. Phys.* **2011**, *13*, 978.
- (39) Wei, Z.; Sun, J.; Li, Y.; Datye, A. K.; Wang, Y. *Chem. Soc. Rev.* **2012**, *41*, 7994.
- (40) Tao, F. *Chem. Commun.* **2012**, *48*, 3812.
- (41) Zhu, Y.; Zhang, S.; Ye, Y.; Zhang, X.; Wang, L.; Zhu, W.; Cheng, F.; Tao, F. *ACS Catal.* **2012**, *2*, 2403.
- (42) Wen, C.; Zhu, Y.; Ye, Y.; Zhang, S.; Cheng, F.; Liu, Y.; Wang, P.; Tao, F. *ACS Nano* **2012**, *6*, 9305.
- (43) Tao, F. *Chem. Commun.* **2012**, *48*, 3812.
- (44) Nashner, M. S.; Frenkel, A. I.; Adler, D. L.; Shapley, J. R.; Nuzzo, R. G. *J. Am. Chem. Soc.* **1997**, *119*, 7760.
- (45) Nashner, M. S.; Frenkel, A. I.; Somerville, D.; Hills, C. W.; Shapley, J. R.; Nuzzo, R. G. *J. Am. Chem. Soc.* **1998**, *120*, 8093.

- (46) Frenkel, A. I.; Hills, C. W.; Nuzzo, R. G. *J. Phys. Chem. B* **2001**, *105*, 12689.
- (47) Sanchez, S. I.; Menard, L. D.; Bram, A.; Kang, J. H.; Small, M. W.; Nuzzo, R. G.; Frenkel, A. I. *J. Am. Chem. Soc.* **2009**, *131*, 7040.
- (48) Salmeron, M.; Schlogl, R. *Surf. Sci. Rep.* **2008**, *63*, 169.
- (49) Tan, B. J.; Klabunde, K. J.; Sherwood, P. M. A. *J. Am. Chem. Soc.* **1991**, *113*, 855.
- (50) Frank Ogletree, D.; Bluhm, H.; Hebenstreit, E. D.; Salmeron, M. *Nucl. Instrum. Methods Phys. Res. Sect. A* **2009**, *601*, 151.
- (51) Grass, M. E.; Zhang, Y.; Butcher, D. R.; Park, J. Y.; Li, Y.; Bluhm, H.; Bratlie, K. M.; Zhang, T.; Somorjai, G. A. *Angew. Chem., Int. Ed.* **2008**, *47*, 8893.
- (52) Wang, Z. L.; Yin, J. S.; Mo, W. D.; Zhang, Z. J. *J. Phys. Chem. B* **1997**, *101*, 6793.
- (53) Zhang, Z. *Ultramicroscopy* **2007**, *107*, 598.
- (54) Zhao, Y.; Feltes, T. E.; Regalbuto, J. R.; Meyer, R. J.; Klie, R. F. *J. Appl. Phys.* **2010**, *108* (6), 063704/1–.
- (55) Shyu, J. Z.; Otto, K. *Appl. Surf. Sci.* **1988**, *32*, 246.
- (56) Boyanov, B. I.; Morrison, T. I. *J. Phys. Chem.* **1996**, *100*, 16318.
- (57) Panagiotopoulou, P.; Kondarides, D. I. *Catal. Today* **2006**, *112*, 49.
- (58) Kalamaras, C. M.; Americanou, S.; Efstathiou, A. M. *J. Catal.* **2011**, *279*, 287.
- (59) Kalamaras, C. M.; Panagiotopoulou, P.; Kondarides, D. I.; Efstathiou, A. M. *J. Catal.* **2009**, *264*, 117.
- (60) Thinon, O.; Rachedi, K.; Diehl, F.; Avenier, P.; Schuurman, Y. *Top. Catal.* **2009**, *52*, 1940.
- (61) Bunluesin, T.; Gorte, R. J.; Graham, G. W. *Appl. Catal., B* **1998**, *15*, 107.
- (62) Xu, W.; Si, R.; Senanayake, S. D.; Llorca, J.; Idriss, H.; Stacchiola, D.; Hanson, J. C.; Rodriguez, J. A. *J. Catal.* **2012**, *291*, 117.
- (63) Panagiotopoulou, P.; Kondarides, D. I. *J. Catal.* **2004**, *225*, 327.
- (64) Kaushik, V. K. Z. *Phys. Chem.—Int. J. Res. Phys. Chem. Chem. Phys.* **1991**, *173*, 105.
- (65) Huizinga, T.; Vantblik, H. F. J.; Vis, J. C.; Prins, R. *Surf. Sci.* **1983**, *135*, 580.
- (66) Liu, P.; Kendelewicz, T.; Brown, G. E. *Surf. Sci.* **1998**, *412–13*, 315.
- (67) Liu, P.; Kendelewicz, T.; Brown, G. E.; Parks, G. A.; Pianetta, P. *Surf. Sci.* **1998**, *416*, 326.
- (68) Liu, P.; Kendelewicz, T.; Nelson, E. J.; Brown, G. E. *Surf. Sci.* **1998**, *415*, 156.